PCCP

PAPER

View Article Online
View Journal | View Issue

Cite this: *Phys. Chem. Chem. Phys.*, 2025, **27**, 16671

Insights into the mechanism of nitrate salt-mediated $MgCO_3$ formation†

Hellen Silva Santos, *[a] Hoang Nguyen, [a] Michael J. Bojdys, [b] Pedram Esmaeili, [a] Juho Antti Sirviö [a] and Paivo Kinnunen [a]

Received 10th April 2025,
Accepted 16th July 2025

DOI: 10.1039/d5cp01372k

rsc.li/pccp

Nitrate salt-mediated carbonation of MgO feedstocks has been extensively studied for CO_2 absorption, but the underlying mechanism remains poorly understood. This study investigates the nucleation and growth of magnesite ($MgCO_3$) in the presence of nitrate salts ($NaNO_3$ and KNO_3) to resolve discrepancies in the carbonation mechanism. Using a simplified sample preparation method, we propose that nitrate salts catalyze $MgCO_3$ formation by (i) lowering the activation energy for brucite ($Mg(OH)_2$) dehydroxylation, (ii) stabilizing Mg^{2+}–CO_3^{2-} ion pairs in nanolayers of water, and (iii) acting as structural nucleation sites due to their crystallographic similarity to magnesite. *In situ* thermogravimetric analyses (TGA-DSC) reveal that the carbonation reaction initiates at ~300 °C, with an exothermic nucleation peak at ~311 °C, indicating that nitrate salts enhance the formation of stable carbonate intermediates. This revised mechanism, where magnesite nucleation occurs *via* water-mediated diffusion of carbonate ions and structural templating by nitrate salts, refines our understanding of $MgCO_3$ crystallization and offer new insights for catalytic carbon mineralization.

Introduction

Impactful carbon capture, utilization, and storage (CCU/S) relies on mineralization pathways to convert CO_2 into stable carbonate phases.[1–4] While calcium-based routes ($CaCO_3$ precipitation) are well understood,[5] the direct precipitation of anhydrous magnesium carbonate ($MgCO_3$) remains a mechanistic challenge.[6–9] Magnesium-rich feedstocks (*e.g.*, Mg-silicate minerals and brine) are abundant in nature, ranking as the eighth-most abundant element in Earth's crust[10] and are also widely available in industrial waste streams such as mine tailings, steel slag, and demolition fines.[11,12] However, despite their theoretical unique potential to store anthropogenic CO_2 on a large scale,[13,14] MgO-based carbonation routes remain kinetically hindered, largely due to the slow formation of anhydrous $MgCO_3$ at ambient conditions and the unclear role of reaction intermediates.[6,11,15]

Alkali metal nitrate salts (*e.g.*, $NaNO_3$, KNO_3) have been proposed as catalysts for CO_2 absorption in MgO-based systems, particularly in pre- or post-combustion CO_2 capture.[4,16–19] Their catalytic effect has been attributed to: (i) lowering the activation energy of magnesite formation,[4] (ii) increasing ion diffusivity due to the dissolution of MgO and CO_2 in molten salts,[20] and (iii) enhancing CO_2 adsorption through their reasonable CO_2 solubility[20] (*e.g.*, 10^{-3} mol L^{-1}/0.04 g L^{-1} for $NaNO_3$ at 300 °C).[21] However, no consensus is found on the mechanism of magnesite formation mediated by the nitrate salts. Two main hypotheses have been proposed: the phase transfer[19] and the interfacial diffusion[16] mechanisms.

The phase transfer mechanism proposes the nucleation and growth of magnesite to occur due to the formation of $[Mg^{2+}\cdots O^{2-}]$ ionic pairs in the molten nitrate salts, which act as phase transfer catalysts, enabling the formation of the carbonate ionic pairs in the gas–solid–liquid triple phase boundaries where the magnesite nucleation is proposed to occur.[4,19] However, the validity of the hypothesis has been contested since it neglects the pre-melting effects[22] and overlooks heterogeneous nucleation.[17,23–25] The interfacial diffusion mechanism postulated the interdiffusion of the carbonate ions through the magnesite product and MgO layer, proposing an initial $MgCO_3$ nucleation in the interface between the molten salt and MgO where the dissolved MgO can react with the absorbed CO_2.[16,23] But the hypothesis has been argued to lack clarity on the transport pathways and explanation for ionic stabilization,[17,18,26–28] and the argument was built under limited conditions, based on the kinetic factors observed for one molar composition of nitrate salts.

Despite the vast body of literature on the topic, it still lacks a unified model to explain the formation of magnesite enabled by

[a] *Fibre and Particle Engineering Research Unit, University of Oulu, Pentti Kaiteran katu 1, PO Box 8000, 90014 Oulu, Finland. E-mail: hellen.silvasantos@oulu.fi; Tel: +358 29 448 2378*
[b] *Center for the Science of Materials Berlin (CSMB), der Humboldt-Universität zu Berlin, Zum Großen Windkanal 2, 12489 Berlin, Germany*

† Electronic supplementary information (ESI) available. See DOI: https://doi.org/10.1039/d5cp01372k

nitrate salts. The direct comparison between studies is challenging due to variations in preparation methods and Mg precursors, hindering comparison between the results and proposed mechanisms (summarized in Table S1, ESI†). For instance, the reported works have high discrepancies on the observed CO_2 uptake, optimal amounts of reagents, and optimal temperatures for the carbonation reaction[17–19,25,27–32] Therefore, a comprehensive model should address the mismatches of results seen between the works, explaining the variable CO_2 uptake aligned with the possible pre-melting effects,[22] wetting properties,[26] relation with surface area,[17,23–25] and heterogeneous nucleation sites.[25]

This study investigates the nucleation and growth mechanism of magnesite in the presence of potassium and sodium nitrate salts. Using a wet mixing approach, *ex situ* characterization, and *in situ* thermogravimetric (TG-DSC) analysis, we explore (i) the catalytic role of nitrate salts in $Mg(OH)_2$ dehydroxylation and CO_2 uptake, (ii) the formation of transient intermediates and the stabilization of Mg^{2+}–CO_3^{2-} ion pairs, and (iii) the structural role of nitrate salts as nucleation templates for magnesite. Our results provide new mechanistic insights into the role of nitrate salts in carbonate mineralization, challenging existing hypotheses and proposing a revised model where magnesite nucleation occurs through water-mediated carbonate diffusion and structural templating by nitrate salts. The findings presented here challenge the phase transfer[19] and interfacial diffusion[16] models by introducing new evidence for the role of nitrate salts as structural nucleation sites, demonstrating the impact of the sample preparation on the carbon extent, and highlighting the variable catalytic efficiency within distinct nitrate salts.

Experimental

Materials & synthesis

The materials were synthesized utilizing analytical grade reagents, namely magnesium oxide (>99%, Sigma-Aldrich, USA), magnesium hydroxide (>99.9%, VWR international, DE), sodium nitrate (>99.5%, Merk, DE), and potassium nitrate (>99%, ThermoFisher Scientific, USA). The syntheses were done by initial wet mixing of 5 g of the Mg precursor with the targeted molar amounts of the nitrate salts (10 and 30 mol%) and adding MilliQ water at the double amount in mass than the total mass of dried reagents. The solid/water ratio was kept consistent for all investigated systems using the wet mixing procedure. All samples were done in triplicates. The slurry was mixed and left to dry for 24 h at 70 °C. It is important to notice that most MgO converts to $Mg(OH)_2$ upon hydration; thus, both systems are expected to have mainly brucite after the addition of water. The carbonation was conducted in a bulky TGA oven (Precisa, prepASH 129, CH), using a CO_2 flow rate of 9 mL min^{-1}. A ramp of 8 min was used to raise the temperature from room temperature to the targeted temperature, and the systems were left reacting for the targeted time. After completion of the reaction, the materials were washed with 500 mL of MilliQ water and 100 mL of isopropanol. The solid products were dried for 24 h at 50 °C.

The main difference between the procedure employed in the current work compared with the wet mixing methods described in the literature is that the dried slurry was submitted to the carbonation step without pre-calcination. The procedure was adjusted as such aiming at minimizing the overall energy consumption of the carbonation route. To assess the role of water in the carbonation of the samples, additional set of samples were prepared without the wet mixing step, mixing the Mg precursors with the nitrate salts in the Thinky mixer for 1 min at 800 rpm and following up with the carbonation of the mixed powders.

Characterization

Mineralogical characterization was performed *via* XRD measurements using a PAnalytical instrument at 40 kV and 45 mA (model X'pert3 MRD), an image plate detector, and Cu Kα radiation (Kα1 = 1.54 Å). The measurements were performed at room temperature (RT) and a scan rate of 0.0167° s^{-1} in the 2θ range of 5°–70° and the step size of 0.017° 2θ/step. Phase identification and quantification were conducted using the HighScore Plus software Version 5.2 (Malvern PanAnalytical, UK) and the PDF-5+ 2020 database. The quantitative XRD analyses were done by Rietveld refinement, using CaF_2 as external standard, determining the amorphous contents through the *G*-factor method.[33,34] The background was fitted using the shifted Chebyshev I function with extended background terms (first 13 terms of the polynomial equation). The refinement of the phases was done by manually refining the scale factors, unit cells, and lattice constants. To avoid high deviations from the initial values of the reference phases, it was allowed a maximum of 5% variation in the reference lattice parameter values as formerly recommended.[35–38] The quantitative analyzes of the XRD patterns are associated with a relative error of ±5–10%. The reference patterns used for phase identification and quantification were the following: magnesite – PDF 04-009-2317,[39] magnesium hydroxide (brucite) – PDF 04-015-9383,[40] sodium nitrate – PDF 04-015-8706,[41] sodium oxide – PDF 01-077-0207,[42] magnesium oxide (periclase) – PDF 00-043-1022,[43] potassium oxide – PDF 00-011-0526,[44] potassium nitrate (*Pnma*) – PDF 04-008-9587,[45] and potassium nitrate ($R\bar{3}m$) – 04-016-7477.[46]

The particle size distribution of the brucite and periclase precursors were evaluated with a laser diffraction particle size analyzer (Beckman Coulter, multi-wavelength, model LS 13 320), utilizing a Turrax liquid module. The samples were prepared by weighing 0.5 g of the sample and dispersing it in 100 mL of isopropanol *via* assisted sonication (9 min at 37 kHz, 100% power). The particle size distribution and specific surface area were calculated with the LS 13320 software (version 5.01), utilizing the Fraunhofer method (assuming the particles as spheric shapes). Table 1 shows the main results extracted from the particle size distribution curves.

The morphologies of the samples were characterized *via* SEM, using a Zeiss (Oberkochen, DE) Ultra Plus field emission scanning electron microscope instrument (secondary electron at an accelerator voltage of 5 kV and a working distance of

Table 1 Results of the particle size distribution analyses of the Mg precursors

Precursor	Brucite	Periclase
Median (μm)	2.9	3.7
Mean (μm)	4.7	6.6
Standard deviation (μm)	4.8	6.7
Specific surface area ($m^2\ g^{-1}$)	3.4	4.0

5–7 mm) where samples were coated with Pt. The carbon contents of the precipitated solids were analyzed using a folded flight path spectrometer for carbon and sulfur analyses (LECO, model CS-230, USA), according to the ASTM standard D4208. The thermal properties of the samples were analyzed through TGA-DSC measurements performed using an SDT 650 model manufactured by TA Instruments; *ca.* 10 mg of powdered samples were calcinated in alumina from 30 °C to 1000 °C with a ramp of 10 °C min^{-1} in a N_2 atmosphere at a flow rate of 100 mL min^{-1}.

In situ carbonation was assessed using a TG-DSC device (Netzsch, STA, 400 PC/PG), adding *ca.* 20 mg of the dried slurries prepared at the ratio of 90 mol% of the Mg precursor and 10 mol% of the nitrate salts, keeping a CO_2 flow of 20 mL min^{-1}, and using a heating ramp of 20 °C min^{-1} from 38 to 300 °C followed by 1 h at 300 °C. The sample carrier temperature calibration was done for four temperature points (In, Bi, Ag, and Au) under a CO_2 flow of 20 mL min^{-1}; thus, adjusting the thermocouple of the sample for the use of the CO_2 gas. The sensitivity calibration was also done under the same CO_2 flow, heating a sapphire glass reference through the thermal range of the device and using the signal and C_p values of sapphire to calibrate the heat flow data (mW mg^{-1}) as a function of the signal detected in the sample carrier (μV mg^{-1}).

Results and discussion

The role of wet-mixing in the sample-preparation step

The variability in the sample preparation methods reported in the literature (Table S1, ESI†) reveals an overlooked part of the process, motivating a systematic investigation into the relevance of the sample preparation for maximized magnesite formation. From the feasibility point of view, the pre-calcination step seemed an unnecessary energy intensive step, whereas the wet mixing method seemed to promote sufficient homogenization of the reagents. That raised relevant questions on the role of water in the pre-treatment step of the samples: would that be a necessary step for maximizing the yields of magnesite formation? Could the wet mixing be avoided to decrease the overall costs when scaling up the route? How does the morphology of the precursors vary in the dried slurry? To shed light on these questions, we investigated the differences between the systems carbonated employing wet or dry mixing as pre-carbonation steps (details in the experimental section). We chose to investigate the systems carbonated with 30 and 10 mol% of nitrate salts, as former works have employed similar ratios.

Fig. 1 shows the XRD patterns of the samples carbonated after wet and dry mixing as well as the quantified magnesite amounts compared between all systems (bottom). The detailed quantitative XRD analyzes are shown in Table S3 (ESI†). The patterns indicate that the samples prepared with the dry mixing had the carbonation reaction hindered in most samples, and a clear increase in the magnesite yield is seen after the wet mixing step. Specially, in the systems prepared with KNO_3, the carbonation after dry mixing was minimal. However, one exception is seen in the system prepared at 70 mol% MgO : 30 mol% $NaNO_3$, where the magnesite yield increased without the wet mixing (Fig. 1e). In this system, it could be argued that the carbonation is facilitated by the high availability of MgO due to combination of factors: lower melting point of $NaNO_3$ than KNO_3 leading to higher amount of the pre-melted salt, and high solubility of MgO:10^{-7} mol kg^{-1} at 300 °C in presence of $NaNO_3$.[23]

We also investigated the absorption of CO_2 in the nitrate salts without the Mg feedstocks. Both nitrate salts were submitted to the carbonation at 300 °C for 1 h, with and without the wet mixing step. The total carbon contents of the samples showed none or minimal CO_2 uptake in the nitrate salts (about 0.06 and 0.05 wt% of carbon in KNO_3 and $NaNO_3$, respectively). Thus, even if the CO_2 solubility increases in presence of the molten salts, the absorption would not occur without the Mg feedstocks.

To assess the reaction progress overtime and the possible formation of additional soluble by-products, we conducted the carbonation of the systems with 70 mol% of the Mg precursor and 30 mol% of the nitrate salts for 6 h at 300 °C and analyzed the carbonation products without the washing step. Fig. S1 (ESI†) shows the XRD patterns of the obtained products and the respective quantitative XRD measurements are shown in Tables S4, S5 (ESI†). The longer carbonation time increases the extent of carbonation, increasing the magnesite contents and completely consuming the brucite contents. Remaining amounts of periclase were noticed in all systems, but at considerably lower contents than the observed in the similar systems carbonated for 1 h.

The results indicated that the wet mixing played an essential role in the carbonation of the MgO precursor, raising further questions: (1) are there remaining water in the system which plays a role in the mechanism of magnesite formation in these systems? And (2) would the amount of trapped water vary according to the molar proportions of nitrate salts?

To investigate these questions, it was chosen to compare the thermal profiles of the dried slurries (after wet mixing) using TGA-DSC measurements (Fig. 2). One main difference between the systems with different nitrate salts is that the occurrence related to the loss of absorbed or coordinated water (60–300 °C) is seen clearly as an endothermic DSC event only in the systems prepared with KNO_3. Overall, the systems showed minor water contents, which is lower than 1 wt% for all systems starting from brucite, about 1.5% for the MgO–$NaNO_3$ systems, and greater for the MgO–KNO_3 systems (*ca.* 3 wt%). The hydration of the MgO precursor to form brucite is also evident, but the

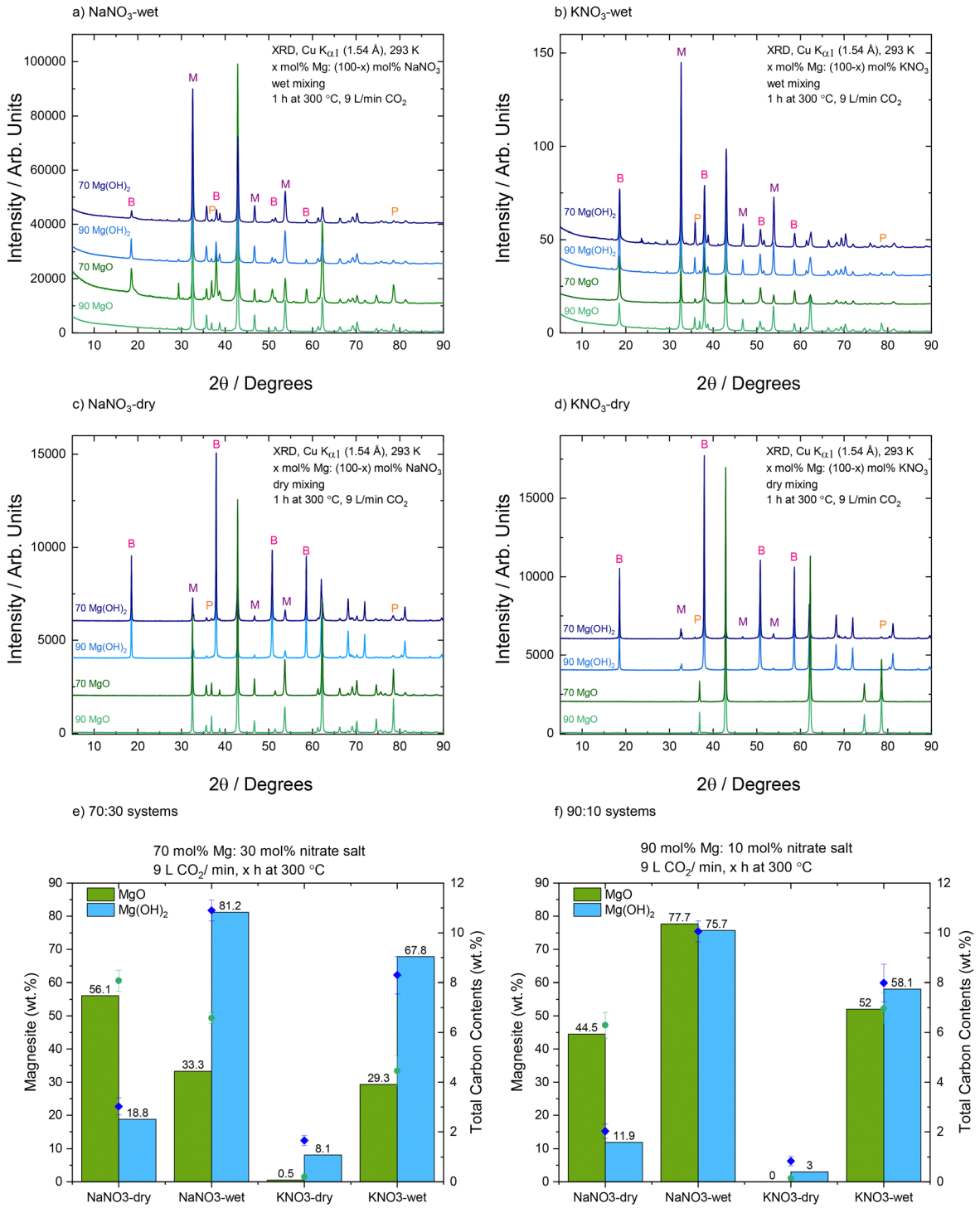

Fig. 1 XRD patterns of the samples prepared at x mol% of Mg and (100 − x) mol% of nitrate salts with (a and b) and without (c and d) wet mixing in the sample preparation prior to the carbonation for 1 h at 300 °C, and comparative column bars graphs (e and f) between the amount of quantified magnesite (left) and total carbon contents (right) in the systems prepared with wet and dry mixing. B = brucite, M = magnesite, and P = periclase.

comparative weight losses with respect to the brucite samples indicate remaining periclase in the dried slurry. The brucite dehydroxylation is reported to occur as an endothermic curve with maximum at 400 °C,[47,48] but in the nitrate salts systems, it is observed at lower temperatures (320 to 350 °C). That indicates a catalytic role of the nitrate salts on the dehydroxylation of brucite, as observed for other additives.[47] Above 400 °C, the observed endothermic events relate to the decomposition of the nitrate salts. These results indicate that absorbed water would have minimal impact on the mechanism of magnesite precipitation, suggesting a major role from the water released by brucite dehydroxylation.

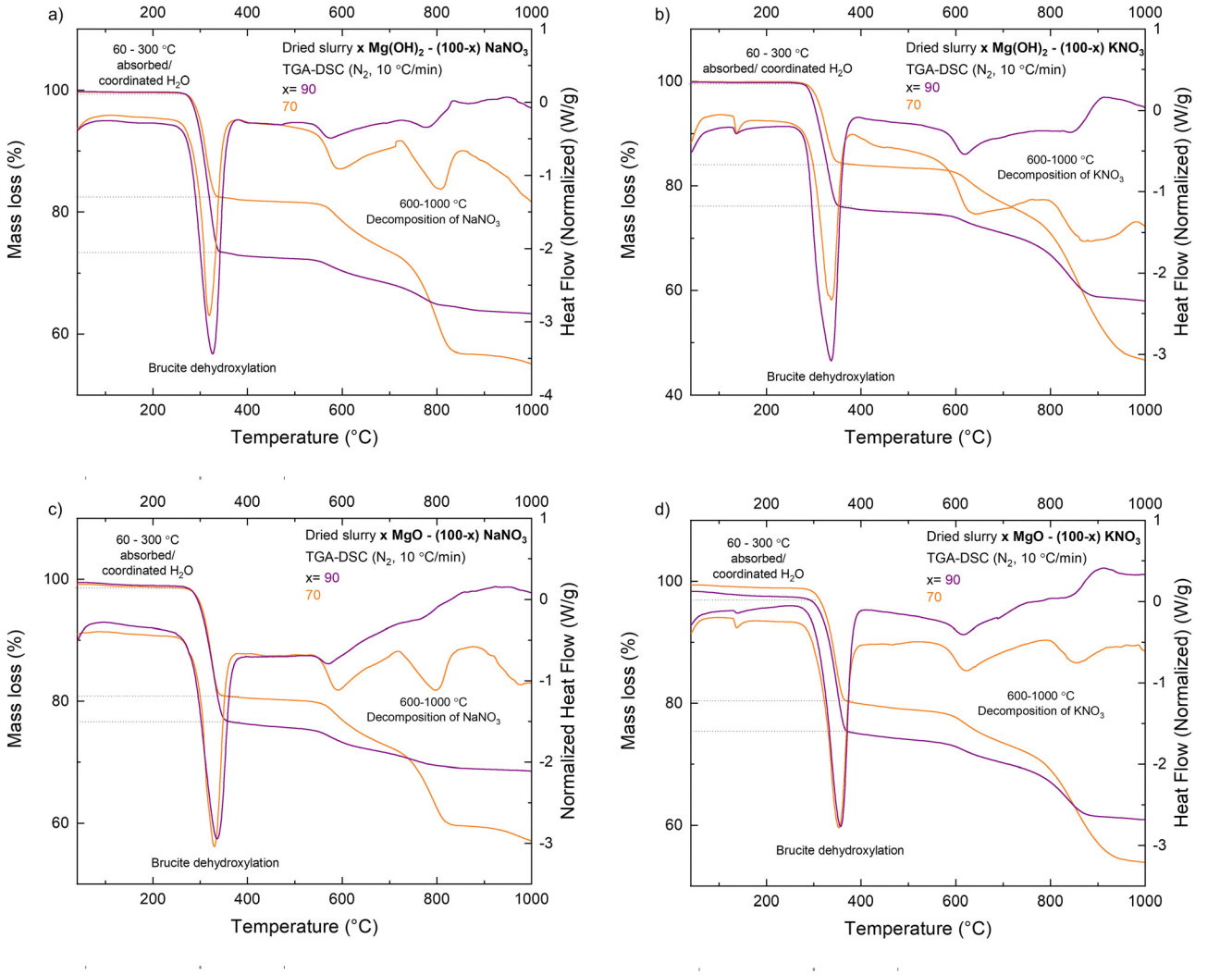

Fig. 2 TGA-DSC of the dried slurries prepared with x mol% of the Mg precursor and (100 − x) mol% of (a, c) $NaNO_3$ and (b, d) KNO_3. All slurries were dried for 24 h at 70 °C prior to the analyses.

Further insights were obtained from the XRD analyses of the dried slurries (Fig. 3 and Table 2), being observed that only a minor fraction of the MgO precursor does not convert to brucite upon hydration, as seen in the TG-DSC results. Interestingly, the increasing contents of nitrate salts relate to decreasing contents of remaining periclase in the system (Table 2), which might relate to differences in MgO solubility. It was noticed that $NaNO_3$ does not undergo phase transformation during wet mixing, whereas KNO_3 is observed as two different crystalline phases. While $NaNO_3$ is observed solely as $R\bar{3}c$ (167) space group,[41] the KNO_3 is observed as two different crystalline phases: *Pnma* (62)[49] as major and $R\bar{3}m$ (166)[50] as minor fraction converted during the wet mixing step (Fig. 4). The formed fraction of KNO_3 as $R\bar{3}m$ was observed to remain in the system after the carbonation for 6 h (Fig. S1 and Table S4, ESI†). This finding is supported by the literature, since KNO_3 is known to undergo different phase transformation under heat; the conversion between the α ↔ β ↔ γ phases happens below 150 °C and melting only at 334 °C.[29,51] $NaNO_3$ has also been reported to occurs as $R\bar{3}m$ space group in certain systems,[41] but it is observed only in the $R\bar{3}c$ conformation in the dried slurries. Previous work investigated the structural evolution of $NaNO_3$ with *in situ* X-ray total scattering and pair distribution function analysis in N_2 atmosphere (Fig. S1, ESI†), observing $NaNO_3$ to remain in the $R\bar{3}c$ symmetry group from RT to 290 °C, when a second order phase transition started to occur, shifting the symmetry from $R\bar{3}c$ to $R\bar{3}m$, and increasing the orientational freedom of the NO_3^- groups in the temperature range from 290 to 308 °C, after which $NaNO_3$ melts and the long-range ordering decreases.[27]

Interestingly, magnesite belongs to the $R\bar{3}c$ symmetry group (Fig. 4), which led us to hypothesize an additional role of the nitrate salts as seeding agents to the magnesite nucleation. In turn, that would also explain why the observed results for the systems with KNO_3 have considerably better performance after wet mixing, being reported to have poor performance in previous investigations. Former studies comparing both salts attributed the poor performance of KNO_3 to its higher melting point, however no wet mixing was employed in these studies, which may explain the reported low yields.[16,22,32] One work has

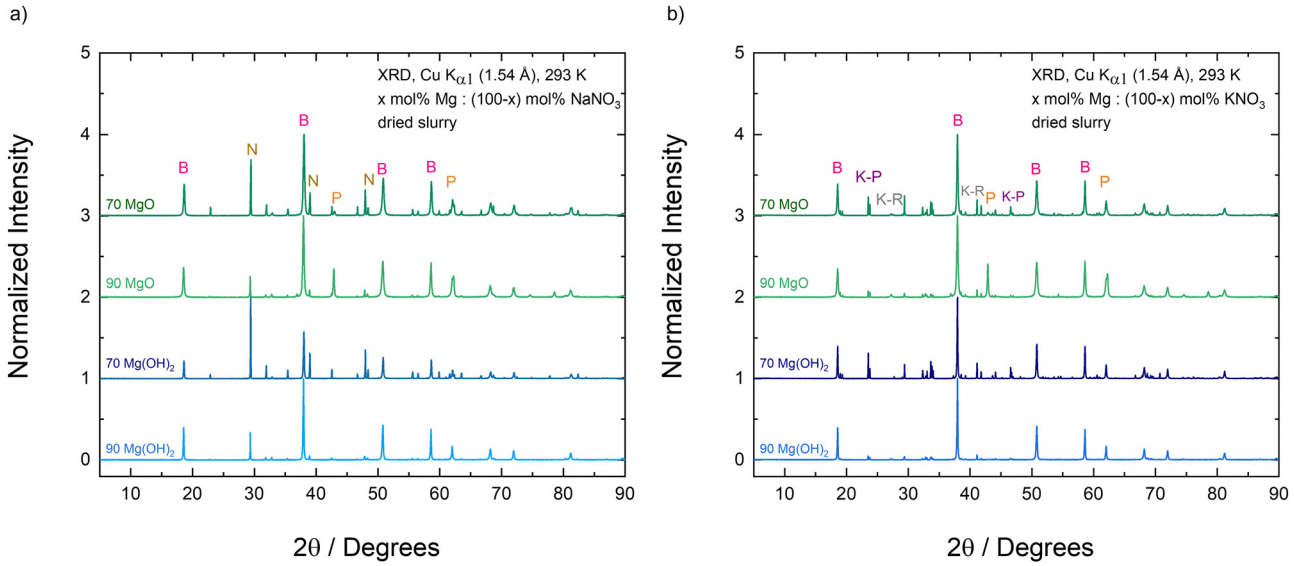

Fig. 3 XRD patterns of the dried slurries prepared using x mol% of the Mg precursor (indicated in the graphs) and y mol% of the nitrate salts: (a) 10 or 30 mol% of $NaNO_3$ and (b) 10 or 30 mol% of KNO_3. All slurries were dried for 24 h at 70 °C prior the analyses. B = brucite, P = periclase, N = sodium nitrate, K-P = potassium nitrate (*pnma*), K-R = potassium nitrate ($R\bar{3}c$).

Table 2 Quantitative XRD analyses of the dried slurries prepared using x mol% of the Mg precursor and 100 − x mol% of the nitrate salts. All slurries were dried for 24 h at 70 °C prior analyses. The measurements have a standard error of ±5–10%. Theoretical values calculated from the mass of the added reagents are shown in Table S2 (ESI)

	Quantified phases: KNO_3 systems (wt%)				
x mol% Mg precursor:100 − x mol% KNO_3	Brucite	Periclase	Potassium nitrate (*Pnma*)	Potassium nitrate ($R\bar{3}m$)	Amorphous
70 MgO:30 KNO_3	69.2	1.5	14.9	1.7	12.7
90 MgO:10 KNO_3	78.6	14.6	4.7	2.1	—
70 $Mg(OH)_2$:30 KNO_3	65.5	—	20.9	0.4	13.2
90 $Mg(OH)_2$:10 KNO_3	90.5	—	8.3	1.3	—

	Quantified phases: $NaNO_3$ systems (wt%)			
x mol% Mg precursor:100 − x mol% $NaNO_3$	Brucite	Periclase	Sodium nitrate ($R\bar{3}c$)	Amorphous
70 MgO:30 $NaNO_3$	67.4	2.1	25.4	5.1
90 MgO:10 $NaNO_3$	77.7	12.6	9.8	—
70 $Mg(OH)_2$:30 $NaNO_3$	48.3	—	48.2	3.5
90 $Mg(OH)_2$:10 $NaNO_3$	85.4	—	14.6	

reported higher CO_2 uptake in the system prepared with KNO_3 than in the system prepared with $NaNO_3$. However, considering the sample pretreatment employed by the authors with autoclave of Mg methoxide, we hypothesize that KNO_3 could have been converted to its $R\bar{3}m$ symmetry group during the sample preparation step employed at that work.[29] However, follow-up validation *via* lattice matching simulations or *in-situ* structural mapping would be needed to confirm the hypothesis.

The SEM images of the dried slurries were also analyzed seeking to evaluate the morphological differences between the Mg precursors employed in the carbonation (Fig. 5). The type of nitrate salt did not affect the morphology of brucite or hydrated MgO, since the phases mixed with both salts, $NaNO_3$ and KNO_3, had identical morphology. However, the morphologies of brucite obtained as reagent grade and the one formed from MgO hydration differ greatly; the latter being observed at considerably smaller particle size (Fig. 5e). The hydration of MgO led to the formation of brucite with distinctive morphology (*i.e.*, thin and flaky shape) compared to hexagonal shape of brucite (reagent grade). This might affect the response of these phases under carbonation as seen previously *e.g.*, in acetate-modified brucite.[47,52] Bork *et al.* observed the formation of pyramidal-shaped micrometer-sized pits on the MgO surface due to the interaction with the molten salts, resulting in a morphology comparable to the obtained one after acidic etching of MgO.[28] However, in the images of the dried slurries, there was no clear presence of etch pits or changes in the morphology of the precursors during wetting process. Therefore, the morphological differences between the samples are associated mainly to the different type of precursors, resulting in a smaller particle

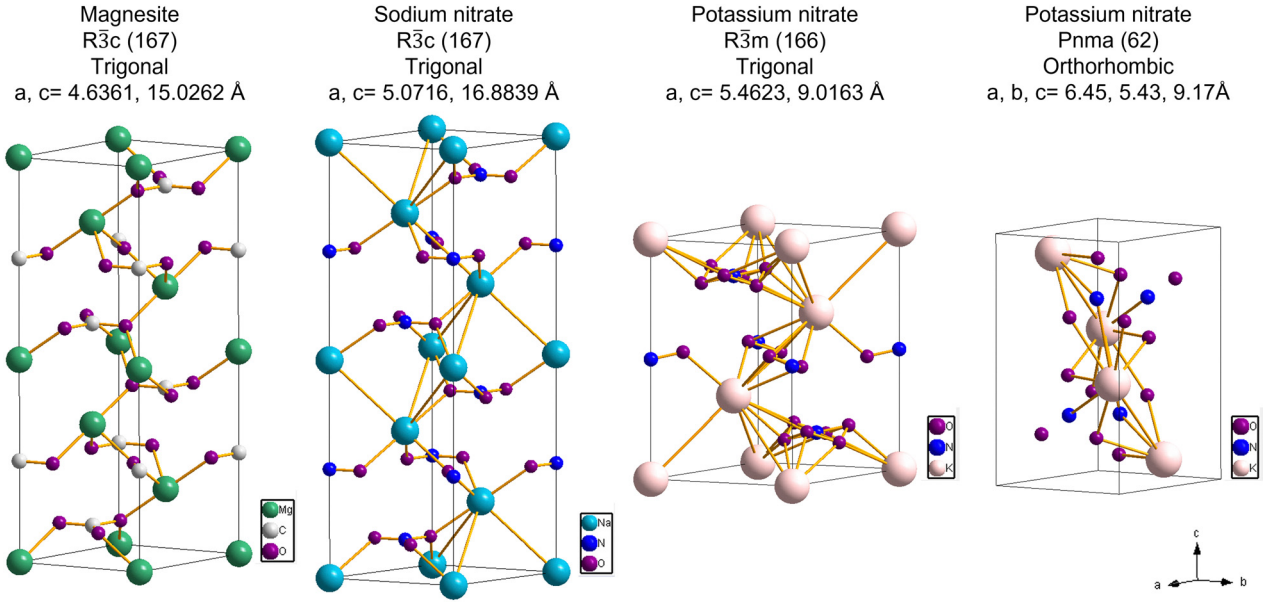

Fig. 4 Representation of the unit cells of magnesite, $NaNO_3$, and KNO_3, aligned in parallel to the *c* axis (as indicated in the coordinates axes). The structures were drawn using the Diamond software, version 5.0.0 Build 45, Crystal Impact GbR, Bonn, Germany.

size in the systems starting from periclase. Thus, we argue that to be one of the factors favoring the higher carbonation extent of the periclase precursor with lower amounts of the molten salts.

To gain deeper insight into the role of the nitrate salts, the carbonation was performed *in situ* using a TG-DSC device with CO_2 flow. The obtained curves are shown as a function of time in Fig. 6. Similarly, the thermal analyses of the dried slurries (Fig. 2), only the systems with KNO_3 showed the initial endothermic event related to the loss of absorbed/coordinated water (Fig. 6c and d). Interestingly, all systems showed an endothermic peak at *ca.* 295 °C and *ca.* 13.2 min, associated with a quick mass loss, which can be attributed to the dehydroxylation of brucite. Indeed, the thermal analyses of the dried slurries in N_2 atmosphere showed the dehydroxylation of brucite occurring as an endothermic peak centered between 320 to 340 °C, which is already shifted *ca.* 50 °C below the predicted value for brucite in N_2 flow due to the presence of the nitrate salts.[27] Thus, we argue that it occurs at lower temperatures in CO_2 flow due to the synergetic effect of the nitrate salts and the CO_2 atmosphere, lowering the energy barrier required for brucite dehydroxylation.

Following that, a sharp exothermic peak linked to a continuous increase in mass is observed, which can be attributed to the nucleation of magnesite. The samples prepared with KNO_3 showed the exothermic peak with maximum at 15 min and 311 °C (Fig. 6c and d), whereas the occurrence appears to be slower in the systems containing $NaNO_3$, being observed at 15.6 and 15.4 min for brucite and periclase, respectively (Fig. 6a and b). The enthalpy associated with the magnesite nucleation was calculated from the area of the exothermic event, being observed to be more exothermic in the systems prepared with $NaNO_3$ (-230.5 and -110.5 J g^{-1} for $Mg(OH)_2$ and MgO, respectively) than in the systems containing KNO_3 (-91.1 and -77.8 J g^{-1} for $Mg(OH)_2$ and MgO, respectively). Dung *et al.* utilized *ab initio* DFT calculations to predict the enthalpy of magnesite formation from periclase: $MgO + CO_2 \leftrightarrow MgCO_3$, $\Delta H_{300\,K} = -1257.86$ J g^{-1},[18,53] roughly one order of magnitude higher compared to our system. While the catalytic effect can be partially offset by the overlapping endothermic dehydroxylation event, the catalytic influence of nitrate salts on brucite dehydroxylation and magnesite growth is clearly supported by the thermal and structural data. However, the calculated enthalpies related to magnesite nucleation are not accurate as the overlap of occurrences cannot be deconvoluted.

The systems prepared with $NaNO_3$ also showed an additional endothermic occurrence, which can be related to the melting of $NaNO_3$ at *ca.* 307 °C (Fig. 6a and b). After the exothermic event linked to the nucleation of magnesite, the DSC curves of all systems appear as a continuous endothermic event related to a continuous mass increase in the TG curve. This observation might suggest that the dehydroxylation of brucite occurs simultaneously with the carbonation reaction and magnesite formation. The TG curves of all systems show that the mass continuously increased, indicating that the carbonation reaction was not complete until the end of the analysis period.

These observations indicate that the magnesite growth and the brucite dehydroxylation continue to occur until the end of the *in situ* measurements. Indeed, the *ex situ* measurements of the systems carbonated for 6 h (Fig. S1 and Tables S4 and S5, ESI†) showed that the carbonation continues to occur, and that the brucite contents were completely consumed after 6 h.

Proposed mechanism for magnesite formation and future perspectives

In view of the observations discussed above, we combined the empirical findings of the current work with the former knowledge available in the literature to propose a mechanism for

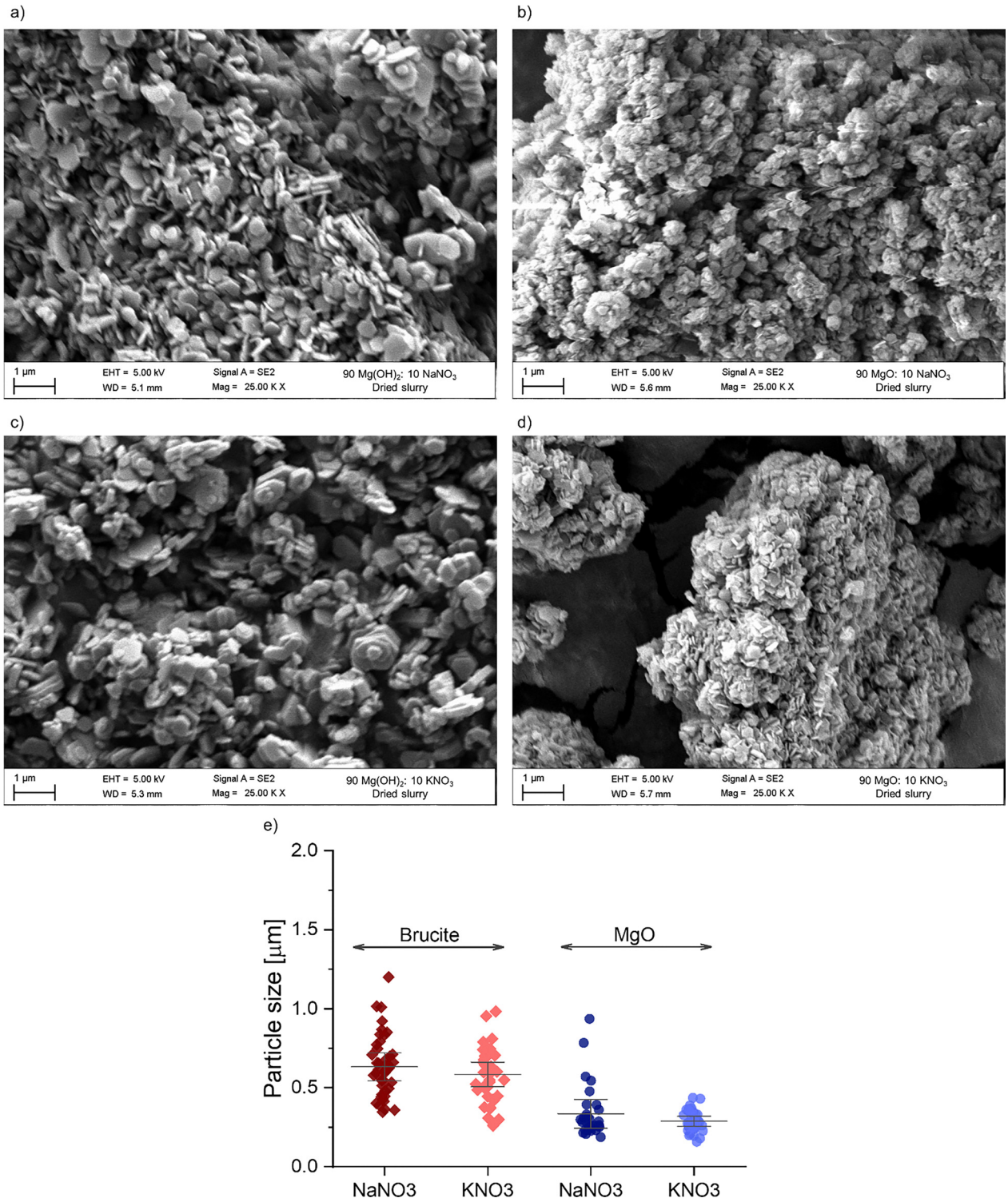

Fig. 5 SEM images of the dried slurries prepared with 90 mol% of the Mg precursor and 10 mol% of the nitrate salts: (a) 90 $Mg(OH)_2$:10 $NaNO_3$, (b) 90 MgO:10 $NaNO_3$, (c) 90 $Mg(OH)_2$:10 KNO_3, and (d) 90 MgO:10 KNO_3. (e) Particle size distribution of the observed brucite crystals, calculated from the SEM image using the ImageJ software (version 1.54, USA).

magnesite formation in our systems. Fig. 7 shows a schematic representation of our understanding on the physico-chemical phenomena involved on both steps – sample preparation and carbonation reaction of magnesite formation.

We observed that the wet mixing method employed to prepare the samples had a strong impact on the yield of magnesite. The starting reagents had statistically similar particle sizes (Table 1), but the SEM images of the dried slurries

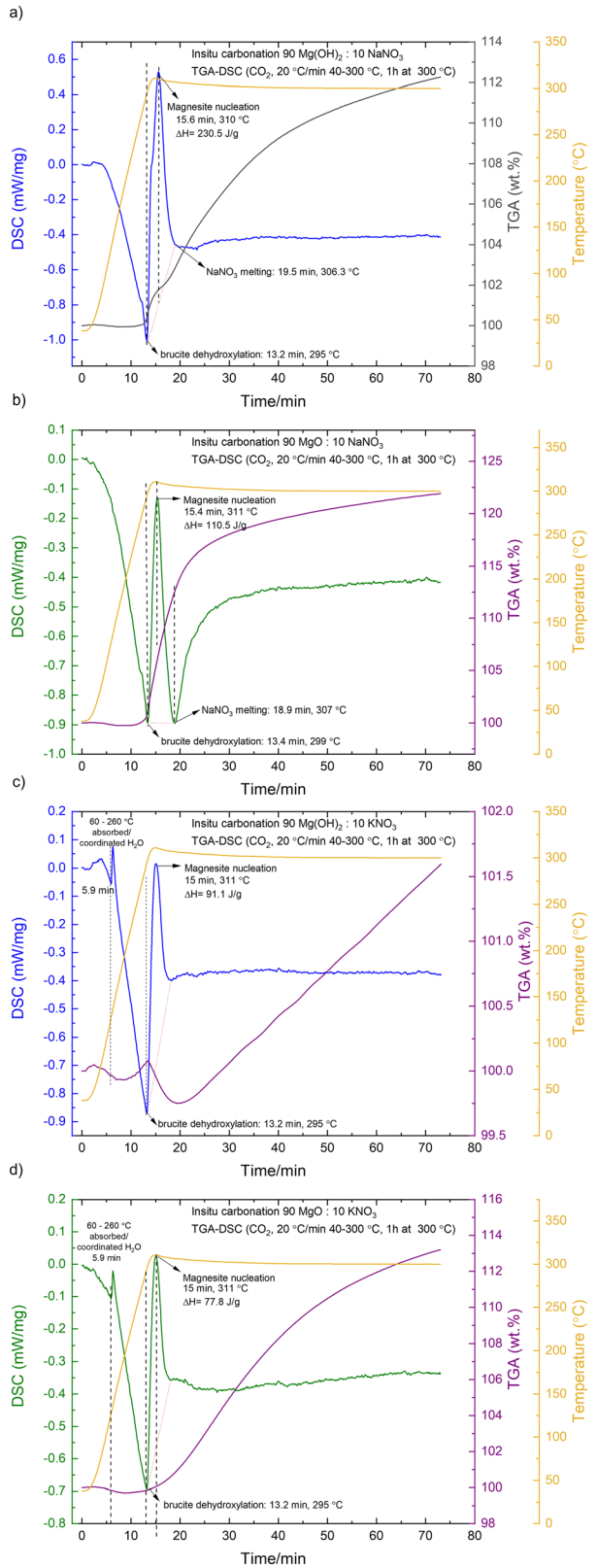

Fig. 6 *In situ* carbonation of the mixtures prepared *via* wet mixing in the ratio of 90 mol% of Mg to 10 mol% of (a, b) $NaNO_3$ and (c, d) KNO_3.

(Fig. 5) indicated that the brucite formed from the hydrated periclase had smaller particle size, thinner layers, and higher degree of packing than the reagent grade brucite. The nitrate salts seemed to enhance the degree of hydration of the periclase reagent (forming brucite), where lower amounts of remaining periclase with decreasing amounts of nitrate salts (Table 2) relate to high magnesite yields (Fig. 1 and Table S2, ESI†). The TG-DSC measurement of the dried slurries (Fig. 2) showed low water contents in the systems which could be hypothesized as nanolayers of water trapped between the reagents. Therefore, the main difference between the systems starting from brucite and periclase was noted as the particle size of the formed brucite and the remaining contents of periclase (Fig. 5 and Table 2). Moreover, *in situ* synchrotron ambient pressure X-ray photoelectron spectroscopy (APXPS) demonstrated that the brucite formed from the hydration of MgO has a metastable hydroxylated interface,[54] which corroborates with the higher overall reactivity observed in that system. Yet, further investigation is needed to understand the impact of the amount of nitrate salts on the morphology of the Mg precursors after the wet mixing procedure.

The nucleation of magnesite has been proposed to occur either homogeneously or heterogeneously, but if the latter is observed, it starts at surface imperfections (*e.g.* edges, dislocations, point defects or nucleation seeds) that assists the formation of stable nuclei at lower energy barrier than the needed for homogeneous nucleation.[17] If the nucleation of magnesite occurs *via* homogeneous nucleation, the availability of the nucleation sites affects the length of the induction period to form a stable nuclei and the growth rate, if an autocatalytic process is assumed.[17] Considering the results observed in the *in-situ* carbonation monitored with TGA-DSC measurements (Fig. 6), our findings agree with the literature that the nucleation seems to occur heterogeneously; otherwise, we would observe strong shifts in the exothermic event related to magnesite formation (among the studied samples). However, we found no evidence of the potential edge pits or surface imperfections that could assist the formation of the nuclei (Fig. 5) as previously suggested,[25] instead we argue that the nitrate salts with similar rhombohedral geometry to magnesite ($R\bar{3}c$ or $R\bar{3}m$) could serve as nucleation seeds for magnesite precipitation.

We propose a mechanism based on the initial arguments of Harada *et al.*,[16] but adjusting it to the information obtained from our observations and combining it with the arguments of Qomi *et al.*[12] about the CO_2 mineralization in nanoscale interfacial water films (Fig. 7). When the gaseous CO_2 contacts the thin water films on the surface, it enhances the absorption by the molten salts and thin water layers.[12,55] The CO_2 is then displaced from the surface, forming either carbonic acid or bicarbonate from the hydroxyl groups available in the water–solid interface. By increasing the temperature, brucite dehydroxylation occurs continuously, regenerating the water layers and increasing the diffusion of the carbonate groups through the feedstock. The high temperatures might also induce a localized transition between the nitrate and nitrite species, facilitating the CO_2 uptake and the formation of the carbonate ions (eqn (1)).[16,17,25,56] In presence of the nitrate salts, the formation of $[Mg^{2+}\cdots O^{2-}]$ ionic pairs are also facilitated

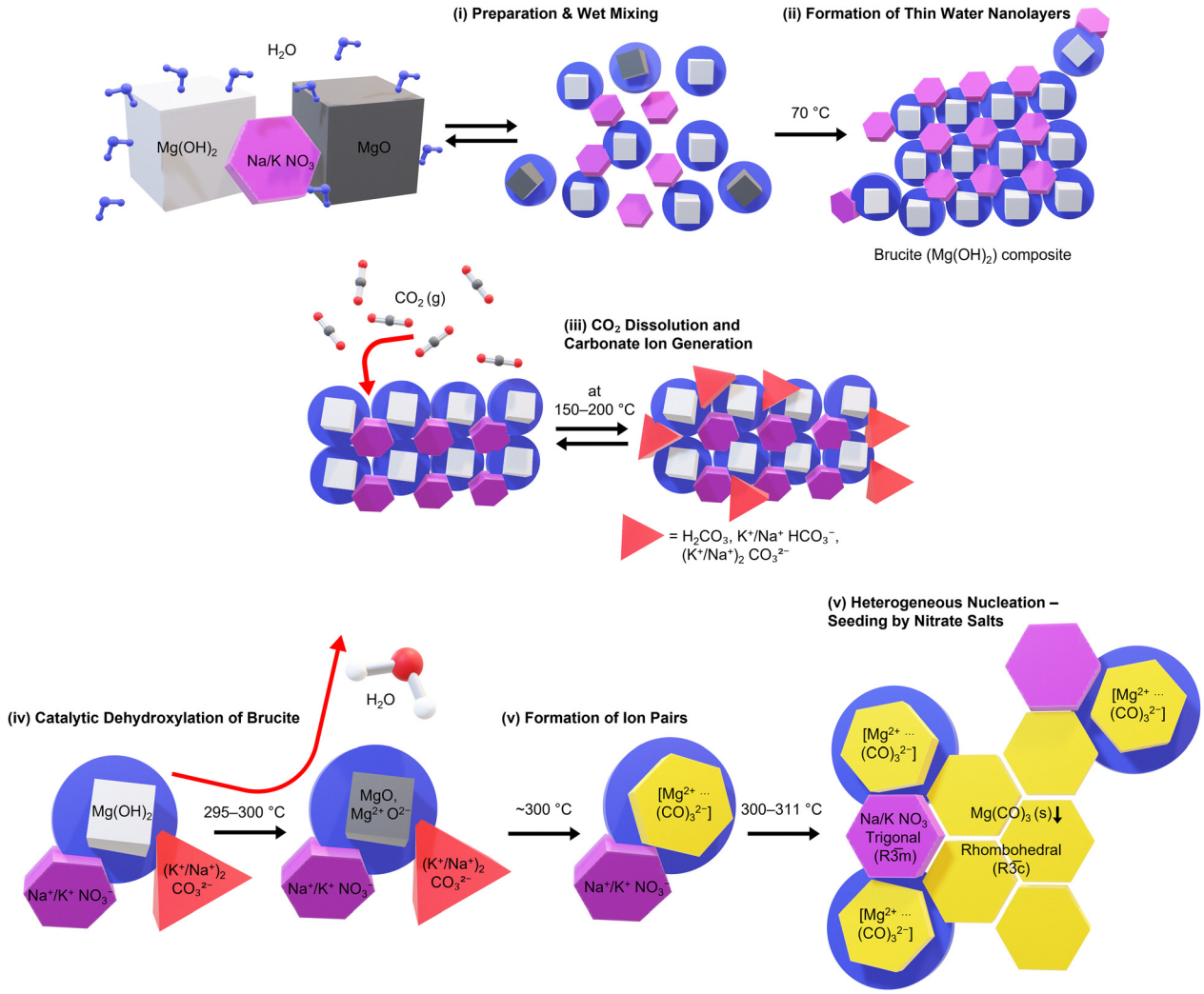

Fig. 7 Proposed mechanism for the nucleation and growth of magnesite in the presence of the nitrate salts, considering the sample preparation *via* wet mixing by using brucite or periclase as precursors.

(eqn (2)),[16–18] enabling the contact between the Mg^{2+} cations and carbonate ions, and the rhombohedral structure of the nitrate salts acts as nucleation seeds for magnesite formation. In a localized high concentrations of Na or K, the formation of double carbonates ($Na_2Mg(CO_3)_2$ or $K_2Mg(CO_3)_2$) will provide additional seeding effect to magnesite nucleation.[17,57]

$$ANO_3(s) + CO_2(g) \xrightarrow{\Delta} [A^+ \cdots NO_3^-] \leftrightarrow [A^+ \cdots NO_2^-] \cdots CO_3^{2-} \quad (1)$$

$$MgO(s) + ANO_3(s) + CO_3^{2-}(aq) \xrightarrow{\Delta} [Mg^{2+} \cdots O^{2-}] + [A^+ \cdots NO_3^-] + CO_3^{2-}(aq) \quad (2)$$

The dissolved ions and ion pairs can be transported in a quasi 2D diffusion in the layers of regenerated water, reaching the nucleation and growth sites potentially *via* a nanofilm-mediated monomer-by-monomer addition mechanism.[12,55,58] The layers of precipitated magnesite do not hinder the diffusion of the carbonate ions, since the molten salts have been shown to migrate to fresh MgO surfaces when magnesite is formed due to the repulsive carbonate surface,[26] also assisting the transport of carbonate ions to the MgO surface. Therefore, the equilibrium between brucite dehydroxylation and periclase formation seems to determine the extent of mass transport on the medium and the distributed formation of water nanolayers to ensure the diffusion of the carbonate ions and further progress of the carbonation reaction.

The results we observed in the current work offer a new perspective on the use of nitrate salts as catalysts for magnesite precipitation, offering the possibility of utilizing the method for magnesite production and its application in construction materials.[59] Remaining questions in the mechanism of the reaction are yet to be elucidated, such as the possible intermediates formed prior to magnesite formation. The proposed mechanism would need further experimental validation with follow-up advanced *in situ* characterization of the carbonated systems. *In situ* Synchrotron XRD measurements could

determine the formation of the intermediate double carbonate species, and the kinetics of brucite dihydroxylation and magnesite nucleation and growth. Thus, we expect to investigate further the phenomenon in upcoming works.

Conclusions

This study investigated the mechanistic role of nitrate salts in mediating the nucleation and growth of magnesite ($MgCO_3$), providing new insights into the carbonation of Mg-based feedstocks. Through a combination of wet mixing and *in situ* thermogravimetric analysis, we demonstrate that nitrate salts act as catalytic agents, facilitating both the dehydroxylation of brucite ($Mg(OH)_2$) and the subsequent precipitation of magnesite. The findings suggest that under the investigated carbonation conditions, the reaction does not proceed purely through direct gas–solid interactions but rather involves an intermediate pathway in which water-mediated ion diffusion and structural templating by nitrate salts play crucial roles.

The results indicate that nitrate salts contribute to magnesite formation in three distinct ways. First, they lower the temperature required for brucite dehydroxylation, thereby increasing the availability of reactive MgO and Mg^{2+} ions for carbonation. This catalytic effect was particularly pronounced for KNO_3, which enhanced the transformation of brucite more significantly than periclase, possibly due to its influence on brucite's layered structure and hydration properties. Second, structural analysis suggests that nitrate salts may act as nucleation templates due to their crystallographic similarity to magnesite. The partial phase transformation of KNO_3 from *Pnma* to $R\bar{3}m$ and of $NaNO_3$ from $R\bar{3}c$ to $R\bar{3}m$ at approximately 300 °C provides a plausible explanation for their ability to facilitate oriented nucleation. The observation that magnesite formation begins before the complete melting of nitrate salts supports the idea that nucleation occurs through structural templating rather than classical molten-phase diffusion.

Third, the presence of water nanolayers in the system appears to serve as a localized transport medium for CO_2 and carbonate species, enhancing ion mobility between the Mg precursor and the growing $MgCO_3$ phase. The formation of these nanolayers, rather than mass transport through bulk molten salts, likely explains why magnesite can precipitate below the expected melting point of the nitrate salts. Furthermore, the correlation between brucite dehydroxylation and magnesite formation suggests that the water released during brucite decomposition facilitates local carbonate ion diffusion, further supporting the role of water-mediated carbonation pathways.

These findings suggest that nitrate salts influence not only the nucleation of magnesite but also its subsequent growth. High magnesite yields were associated with larger particle sizes, indicating that nitrate salts may affect crystal growth kinetics in addition to initiating nucleation. The proposed mechanism, in which magnesite formation is mediated by water layers and nitrate salts acting as structural templates, provides a revised framework that reconciles inconsistencies in previous studies.

Follow-up work should investigate how the amount of water employed in the sample preparation affects the reaction yield, and in-depth characterization of the systems are needed to broaden the understanding on the impact of the amount of molten salts on the precursors morphology, the formation of intermediates and the kinetics of the systems. While our results strongly support a catalytic and structural role of nitrate salts in magnesite formation, further studies employing *in situ* characterization and molecular simulations will be necessary to confirm the nucleation templating hypothesis and to clarify the transient phases involved.

Table 3 Authors' detailed contribution to the work

Contributor Role	H.S.S.	H.N.	M.J.B.	P.E.	J.A.S.	P.K.
Conceptualization	■	■			■	■
Methodology	■	■			■	■
Software	■	■				
Validation	■	■	■		■	■
Formal Analysis	■	■	■			■
Investigation	■	■	■	■		■
Resources	■					■
Data Curation	■	■	■			■
Writing – Original Draft	■		■			■
Writing – Review & Editing	■	■	■	■	■	■
Visualization	■	■			■	■
Supervision						■
Project Administration						■

Author contributions

The contributions to this work, according to the CRediT statement is detailed in Table 3.

Conflicts of interest

All authors declare no conflict of interest.

Data availability

Following the FAIR data principles, all data presented in the current publication is available at QVAIN/IDA server with a permanent DOI address (**https://doi.org/10.23729/fd-f090e2bc-7274-3831-a9a4-2383d2948043**).

Acknowledgements

H. S. S., P. E. and P. K. acknowledge the financial support from the Research Council of Finland (funding decision 347183). P. K. and H. N. acknowledges financial support from the Research Council of Finland (grant 329477 and 354767) and

from the University of Oulu & the Research Council of Finland Profi5 (326291). The authors acknowledge Jasmiini Tornberg for the sharp tunning of the graphical abstract. Special thanks to Tommi Kokkonen for performing the *in situ* TG-DSC measurements. HSS and P. E. also acknowledge Elisa Wirkkala and Jarno Karvonen for their assistance with the laboratory work.

References

1 G. Faber, A. Ruttinger, T. Strunge, T. Langhorst, A. Zimmermann, M. van der Hulst, F. Bensebaa, S. Moni and L. Tao, Adapting Technology Learning Curves for Prospective Techno-Economic and Life Cycle Assessments of Emerging Carbon Capture and Utilization Pathways, *Front. Clim.*, 2022, **4**, 820261, DOI: **10.3389/fclim.2022.820261**.

2 D. Hills, C. Nimisha Tripathi and P. J. Carey, Managed Pathways for CO_2 Mineralisation: Analogy with Nature and Potential Contribution to CCUS-Led Reduction Targets, *Faraday Discuss.*, 2021, **230**(0), 152–171, DOI: **10.1039/D0FD00142B**.

3 C. Unluer, Carbon Dioxide Sequestration in Magnesium-Based Binders, *Carbon Dioxide Sequestration in Cementitious Construction Materials*, 2018, pp. 129–173, DOI: **10.1016/B978-0-08-102444-7.00007-1**.

4 Y. Shen, Molten Salt-Mediated Carbon Capture and Conversion, *Fuel*, 2023, **339**, 127473, DOI: **10.1016/j.fuel.2023.127473**.

5 L. M. Seymour, J. Maragh, P. Sabatini, M. Di Tommaso, J. C. Weaver and A. Masic, Hot Mixing: Mechanistic Insights into the Durability of Ancient Roman Concrete, *Sci. Adv.*, 2023, **9**(1), eadd1602, DOI: **10.1126/sciadv.add1602**.

6 H. S. Santos, H. Nguyen, F. Venâncio, D. Ramteke, R. Zevenhoven and P. Kinnunen, Mechanisms of Mg Carbonates Precipitation and Implications for CO_2 Capture and Utilization/Storage, *Inorg. Chem. Front.*, 2023, **10**, 2507–2546, DOI: **10.1039/D2QI02482A**.

7 D. Toroz, F. Song, G. A. Chass and D. Di Tommaso, New Insights into the Role of Solution Additive Anions in Mg2+ Dehydration: Implications for Mineral Carbonation, *CrystEngComm*, 2021, **23**, 4896–4900, DOI: **10.1039/D1CE00052G**.

8 J. M. Gregg, D. L. Bish, S. E. Kaczmarek and H. G. Machel, Mineralogy, Nucleation and Growth of Dolomite in the Laboratory and Sedimentary Environment: A Review, *Sedimentology*, 2015, **62**(6), 1749–1769, DOI: **10.1111/SED.12202**.

9 E. Bernard, B. Lothenbach, D. Rentsch, A. German and F. Winnefeld, Effect of Carbonates on the Formation of Magnesium Silicate Hydrates, *Mater. Struct.*, 2022, **55**, 183.

10 H. W. Leimer and H. Wayne Leimer, *Homepage. Abundances of Chemical Elements in the Earth's Crust*, **https://sites.tntech.edu/hwleimer/geol-1040/geol-1040-lecture/abundances-of-chemical-elements-in-the-earths-crust/** (accessed 2023-04-23).

11 G. Gadikota, Carbon Mineralization Pathways for Carbon Capture, Storage and Utilization, *Commun. Chem.*, 2021, **4**(1), 1–5, DOI: **10.1038/s42004-021-00461-x**.

12 M. J. Abdolhosseini Qomi, Q. R. S. Miller, S. Zare, H. T. Schaef, J. P. Kaszuba and K. M. Rosso, Molecular-Scale Mechanisms of CO_2 Mineralization in Nanoscale Interfacial Water Films, *Nat. Rev. Chem.*, 2022, **6**(9), 598–613, DOI: **10.1038/s41570-022-00418-1**.

13 A. Scott, C. Oze, V. Shah, N. Yang, B. Shanks, C. Cheeseman, A. Marshall and M. Watson, Transformation of Abundant Magnesium Silicate Minerals for Enhanced CO_2 Sequestration, *Commun. Earth Environ.*, 2021, **2**(1), 1–6, DOI: **10.1038/s43247-021-00099-6**.

14 E. Van Roijen, S. A. Miller and S. J. Davis, Building Materials Could Store More than 16 Billion Tonnes of CO_2 Annually, *Science*, 2025, **387**(6730), 176–182, DOI: **10.1126/science.adq8594**.

15 G. Gadikota, Multiphase Carbon Mineralization for the Reactive Separation of CO_2 and Directed Synthesis of H_2, *Nat. Rev. Chem.*, 2020, **4**(2), 78–89, DOI: **10.1038/s41570-019-0158-3**.

16 T. Harada, F. Simeon, E. Z. Hamad and T. A. Hatton, Alkali Metal Nitrate-Promoted High-Capacity MgO Adsorbents for Regenerable CO_2 Capture at Moderate Temperatures, *Chem. Mater.*, 2015, **27**(6), 1943–1949, DOI: **10.1021/cm503295g**.

17 M. Rekhtina, M. Krödel, Y.-H. Wu, A. Kierzkowska, F. Donat, P. M. Abdala and C. R. Müller, Deciphering the Structural Dynamics in Molten Salt–Promoted MgO-Based CO_2 Sorbents and Their Role in the CO_2 Uptake, *Sci. Adv.*, 2023, **9**, eadg5690, DOI: **10.1126/sciadv.adg5690**.

18 M. Rekhtina, A. Bugaev, M. T. Dunstan, A. Dal Pozzo, M. Nadjafi, C. Borca, T. Huthwelker, P. M. Abdala and C. R. Müller, Probing the Local Structure of Na in $NaNO_3$-Promoted, MgO-Based CO_2 Sorbents via X-Ray Absorption Spectroscopy, *Chem. Mater.*, 2023, **35**(23), 10060–10069, DOI: **10.1021/acs.chemmater.3c02077**.

19 K. Zhang, X. S. Li, W.-Z. Li, A. Rohatgi, Y. Duan, P. Singh, L. Li and D. L. King, Phase Transfer-Catalyzed Fast CO_2 Absorption by MgO-Based Absorbents with High Cycling Capacity, *Adv. Mater. Interfaces*, 2014, **1**(3), 1400030, DOI: **10.1002/admi.201400030**.

20 R. N. Kust, Carbonate Ion Dissociation in Fused Alkali Nitrates, *Inorg. Chem.*, 1964, **3**(7), 1035–1036, DOI: **10.1021/ic50017a027**.

21 E. Sada, S. Katoh, H. Beniko, H. Yoshii and M. Kayano, Solubility of Carbon Dioxide in Molten Salts, *J. Chem. Eng. Data*, 1980, **25**(1), 45–47, DOI: **10.1021/je60084a019**.

22 K. Zhang, X. S. Li, H. Chen, P. Singh and D. L. King, Molten Salt Promoting Effect in Double Salt CO_2 Absorbents, *J. Phys. Chem. C*, 2016, **120**(2), 1089–1096, DOI: **10.1021/acs.jpcc.5b10729**.

23 T. Harada and T. A. Hatton, Colloidal Nanoclusters of MgO Coated with Alkali Metal Nitrates/Nitrites for Rapid, High Capacity CO_2 Capture at Moderate Temperature, *Chem. Mater.*, 2015, **27**(23), 8153–8161, DOI: **10.1021/acs.chemmater.5b03904**.

24 L. Wang, Z. Zhou, Y. Hu, Z. Cheng and X. Fang, Nanosheet MgO-Based CO_2 Sorbent Promoted by Mixed-Alkali-Metal Nitrate and Carbonate: Performance and Mechanism, *Ind. Eng. Chem. Res.*, 2017, **56**(20), 5802–5812, DOI: **10.1021/acs.iecr.7b00483**.

25 X. Zhao, G. Ji, W. Liu, X. He, E. J. Anthony and M. Zhao, Mesoporous MgO Promoted with $NaNO_3$/NaNO2 for Rapid and High-Capacity CO_2 Capture at Moderate Temperatures, *Chem. Eng. J.*, 2018, **332**, 216–226, DOI: 10.1016/j.cej.2017.09.068.

26 S.-I. Jo, Y.-I. An, K.-Y. Kim, S.-Y. Choi, J.-S. Kwak, K.-R. Oh and Y.-U. Kwon, Mechanisms of Absorption and Desorption of CO_2 by Molten $NaNO_3$-Promoted MgO, *Phys. Chem. Chem. Phys.*, 2017, **19**(8), 6224–6232, DOI: 10.1039/C6CP07787K.

27 M. Rekhtina, A. Dal Pozzo, D. Stoian, A. Armutlulu, F. Donat, M. V. Blanco, Z.-J. Wang, M.-G. Willinger, A. Fedorov, P. M. Abdala and C. R. Müller, Effect of Molten Sodium Nitrate on the Decomposition Pathways of Hydrated Magnesium Hydroxycarbonate to Magnesium Oxide Probed by in Situ Total Scattering, *Nanoscale*, 2020, **12**(31), 16462–16473, DOI: 10.1039/D0NR01760D.

28 A. H. Bork, M. Rekhtina, E. Willinger, P. Castro-Fernández, J. Drnec, P. M. Abdala and C. R. Müller, Peering into Buried Interfaces with X-Rays and Electrons to Unveil $MgCO_3$ Formation during CO_2 Capture in Molten Salt-Promoted MgO, *Proc. Natl. Acad. Sci. U. S. A.*, 2021, **118**(26), e2103971118, DOI: 10.1073/pnas.2103971118.

29 A.-T. Vu, Y. Park, P. R. Jeon and C.-H. Lee, Mesoporous MgO Sorbent Promoted with KNO_3 for CO_2 Capture at Intermediate Temperatures, *Chem. Eng. J.*, 2014, **258**, 254–264, DOI: 10.1016/j.cej.2014.07.088.

30 K.-R. Oh, K.-Y. Kim, J.-S. Kwak, G. Atila and Y.-U. Kwon, Syntheses of $MgCO_3$ and $Na_2Mg(CO_3)_2$ through Solid-Gas Reactions Mediated by Alkali Nitrates, *J. Solid State Chem.*, 2018, **263**, 224–230, DOI: 10.1016/j.jssc.2018.04.025.

31 H. Lee, M. L. T. Triviño, S. Hwang, S. H. Kwon, S. G. Lee, J. H. Moon, J. Yoo and J. G. Seo, In Situ Observation of Carbon Dioxide Capture on Pseudo-Liquid Eutectic Mixture-Promoted Magnesium Oxide, *ACS Appl. Mater. Interfaces*, 2018, **10**(3), 2414–2422, DOI: 10.1021/acsami.7b14256.

32 A. Dal Pozzo, A. Armutlulu, M. Rekhtina, P. M. Abdala and C. R. Müller, CO 2 Uptake and Cyclic Stability of MgO-Based CO 2 Sorbents Promoted with Alkali Metal Nitrates and Their Eutectic Mixtures, *ACS Appl. Energy Mater.*, 2019, **2**(2), 1295–1307, DOI: 10.1021/acsaem.8b01852.

33 B. H. O'Connor and M. D. Raven, Application of the Rietveld Refinement Procedure in Assaying Powdered Mixtures, *Powder Diffr.*, 1988, **3**(1), 2–6, DOI: 10.1017/S0885715600013026.

34 D. Jansen, C. Stabler, F. Goetz-Neunhoeffer, S. Dittrich and J. Neubauer, Does Ordinary Portland Cement Contain Amorphous Phase? A Quantitative Study Using an External Standard Method, *Powder Diffr.*, 2011, **26**(1), 31–38, DOI: 10.1154/1.3549186.

35 R. Snellings, A. Bazzoni and K. Scrivener, The Existence of Amorphous Phase in Portland Cements: Physical Factors Affecting Rietveld Quantitative Phase Analysis, *Cem. Concr. Res.*, 2014, **59**, 139–146, DOI: 10.1016/j.cemconres.2014.03.002.

36 R. Snellings, *A Practical Guide to Microstructural Analysis of Cementitious Materials*, ed. K. Scrivener, R. Snellings and B. Lothenbach, CRC Press, 1st edn, 2018, DOI: 10.1201/b19074.

37 F. Winnefeld, F. Läng and A. Leemann, Pozzolanic Reaction of Carbonated Wollastonite Clinker, *J. Adv. Concr. Technol.*, 2023, **21**(8), 631–642, DOI: 10.3151/jact.21.631.

38 F. Winnefeld, J. Kaufmann, R. Loser and A. Leemann, Influence of Shotcrete Accelerators on the Hydration of Cement Pastes and Their Impact on Sulfate Resistance, *Constr. Build. Mater.*, 2021, **266**, 120782, DOI: 10.1016/j.conbuildmat.2020.120782.

39 S. Göttlicher and A. Vegas, Electron-Density Distribution in Magnesite (MgCO 3), *Acta Crystallogr., Sect. B: Struct. Sci.*, 1988, **44**(4), 362–367, DOI: 10.1107/S0108768188002332.

40 M. Catti, G. Ferraris, S. Hull and A. Pavese, Static Compression and H Disorder in Brucite, Mg(OH)2, to 11 GPa: A Powder Neutron Diffraction Study, *Phys. Chem. Miner.*, 1995, **22**(3), 200–206, DOI: 10.1007/BF00202300.

41 S. M. Antao, I. Hassan, W. H. Mulder and P. L. Lee, The R3c to R3m Transition in Nitratine, $NaNO_3$, and Implications for Calcite, $CaCO_3$, *Phys. Chem. Miner.*, 2008, **35**(10), 545–557, DOI: 10.1007/s00269-008-0232-8.

42 M. Ziegler, M. Rosenfeld, W. Kaenzig and P. Fischer, Strukturuntersuchungen an Alkalihyperoxiden, *Helv. Phys. Acta*, 1976, **49**, 57.

43 S. Sasaki, K. Fujino and Y. Takéuchi, X-Ray Determination of Electron Density Distributions in Oxides, MgO, MnO, CoO, and NiO, and Atomic Scattering Factors of Their Constituent Atoms, *Proc. Japan Acad.*, 1979, **55**(ser. B), 43.

44 Z. Zhdanova, K_2O, *Zh. Fiz. Khim.*, 1951, **25**, 100.

45 F. M. and F. P., Determination Des Constantes Elastiques de KNO_3, Phase II, *C. R. Seances Acad. Sci., Ser. B*, 1971, **272**, 848–850.

46 N. Guillou, J. P. Auffredic and D. Louër, An Unexpected Double Valence Change for Cerium during the Thermal Decomposition of $CeK_2(NO_3)_6$, *J. Solid State Chem.*, 1995, **115**(1), 295–298, DOI: 10.1006/jssc.1995.1136.

47 N. Kamala Ilango, H. Nguyen, A. German, F. Winnefeld and P. Kinnunen, Role of Magnesium Acetate in Hydration and Carbonation of Magnesium Oxide-Based Cements, *Cem. Concr. Res.*, 2024, **175**, 107357, DOI: 10.1016/j.cemconres.2023.107357.

48 H. Ren, Z. Chen, Y. Wu, M. Yang, J. Chen, H. Hu and J. Liu, Thermal Characterization and Kinetic Analysis of Nesquehonite, Hydromagnesite, and Brucite, Using TG–DTG and DSC Techniques, *J. Therm. Anal. Calorim.*, 2014, **115**(2), 1949–1960, DOI: 10.1007/s10973-013-3372-0.

49 F. Michard and F. Plicque, Determination Des Constantes Elastiques de KNO_3, Phase II, *C. R. Seances Acad. Sci., Ser. B*, 1971, **272**, 848–850.

50 E. J. Freney, L. A. J. Garvie, T. L. Groy and P. R. Buseck, Growth and Single-Crystal Refinement of Phase-III Potassium Nitrate, KNO_3, *Acta Crystallogr. Sect. B Struct. Sci.*, 2009, **65**(6), 659–663, DOI: 10.1107/S0108768109041019.

51 H. M. Lu and J. R. Hardy, First-Principles Study of Phase Transitions in KNO_3, *Phys. Rev. B: Condens. Matter Mater. Phys.*, 1991, **44**(14), 7215–7224, DOI: 10.1103/PhysRevB.44.7215.

52 Z. Du and C. Unluer, Modification of Magnesium Hydroxide for Improved Performance in CO_2 Sequestration, *Cem. Concr. Res.*, 2024, **177**, 107418, DOI: 10.1016/j.cemconres.2023.107418.

53 Y. Duan, K. Zhang, X. S. Li, D. L. King, B. Li, L. Zhao and Y. Xiao, Ab Initio Thermodynamic Study of the CO_2 Capture Properties of M_2CO_3 (M = Na, K)- and $CaCO_3$-Promoted MgO Sorbents Towards Forming Double Salts, *Aerosol Air Qual. Res.*, 2014, **14**(2), 470–479, DOI: **10.4209/aaqr.2013.05.0178**.

54 J. T. Newberg, Surface Thermodynamics and Kinetics of MgO(100) Terrace Site Hydroxylation, *J. Phys. Chem. C*, 2014, **118**(50), 29187–29195, DOI: **10.1021/jp5052613**.

55 M. F. Ruiz-Lopez, J. S. Francisco, M. T. C. Martins-Costa and J. M. Anglada, Molecular Reactions at Aqueous Interfaces, *Nat. Rev. Chem.*, 2020, **4**(9), 459–475, DOI: **10.1038/s41570-020-0203-2**.

56 Y. Qiao, J. Wang, Y. Zhang, W. Gao, T. Harada, L. Huang, T. A. Hatton and Q. Wang, Alkali Nitrates Molten Salt Modified Commercial MgO for Intermediate-Temperature CO_2 Capture: Optimization of the Li/Na/K Ratio, *Ind. Eng. Chem. Res.*, 2017, **56**(6), 1509–1517, DOI: **10.1021/acs.iecr.6b04793**.

57 E. Willinger, F. Donat, C. Colbea, M. Mirolo and M. Willinger, *The Interplay between Carbonate Phases in Promoted Carbonation of MgO*, *Chemrxiv*, 2025, preprint, DOI: **10.26434/chemrxiv-2025-clc28**.

58 J. J. De Yoreo, P. U. P. A. Gilbert, N. A. J. M. Sommerdijk, R. L. Penn, S. Whitelam, D. Joester, H. Zhang, J. D. Rimer, A. Navrotsky, J. F. Banfield, A. F. Wallace, F. M. Michel, F. C. Meldrum, H. Cölfen and P. M. Dove, Crystallization by Particle Attachment in Synthetic, Biogenic, and Geologic Environments, *Science*, 2015, **349**(6247), aaa6760, DOI: **10.1126/science.aaa6760**.

59 W. Wang, Y. Xu, Q. Lv and Y. Zhang, Influence of Magnesite/Limestone Addition on the Hydration Characteristics of Ternary Slag Cement Systems, *Constr. Build. Mater.*, 2024, **449**, 138249, DOI: **10.1016/j.conbuildmat.2024.138249**.

